Proceedings of ASME 2011 9th International Conference on Nanochannels, Microchannels, and Minichannels
ICNMM2011
June 19-22, 2011, Edmonton, Alberta, CANADA

ICNMM2011-58296

PERSPECTIVES ON THE SIMULATION OF MICRO GAS AND NANO LIQUID FLOWS

Jason M. Reese
Department of Mechanical Engineering
University of Strathclyde
Glasgow G1 1XJ, UK
email: jason.reese@strath.ac.uk

William D. Nicholls
Department of Mechanical Engineering
University of Strathclyde
Glasgow G1 1XJ, UK
email: william.nicholls@strath.ac.uk

ABSTRACT

Micro- and nano-scale fluid systems can behave very differently from their macro-scale counterparts. Remarkably, there is no sufficiently accurate, computationally efficient, and — most importantly — generally agreed fluid dynamic model that encapsulates all of this important behaviour. The only thing that researchers can agree on is that the conventional Navier-Stokes fluid equations are unable to capture the unique complexity of these often locally non-thermodynamic-equilibrium flows. Here, we outline recent work on developing and exploring new models for these flows, highlighting, in particular, slip flow as a quintessential non-equilibrium (or sub-continuum) phenomenon. We describe the successes and failures of various hydrodynamic and molecular models in capturing the non-equilibrium flow physics in current test applications in micro and nano engineering, including the aerodynamic drag of a sphere in a rarefied gas, and the flow of water along carbon nanotubes.

INTRODUCTION

The set of Navier-Stokes-Fourier (NSF) equations, with no-velocity-slip and no-temperature-jump conditions at bounding surfaces, is the traditional model for the transfer of heat and momentum in fluid flows. While it has proven successful for flows ranging from liquids in capillaries to the atmosphere of planets, remarkably it can be a poor predictor when the flow system is either very small (i.e. in micro/nano devices) or very low pressure (e.g. high-altitude air vehicles, spacecraft re-entry), or if the process depends on interactions at the molecular level (e.g. protein folding). This is despite the flows being very typically laminar in such conditions, so simpler in a conventional sense. For example, measured gas flow rates in micro channels are typically a factor of two larger than expected, and drag on a micro sphere is a similar factor smaller [1]. At the nano scale, surface effects such as hydrophobicity, wetting and electrokinetics dominate, and lead to unexpectedly high liquid transport rates in, e.g., carbon nanotubes that different experimental groups not only cannot fully explain but also fail to agree on.

These predictive failures arise from a limiting assumption underlying conventional fluid mechanics: scale-separation — macroscopic flow behaviour is assumed to be independent of the microscopic dynamics of the fluid material [2]. The conventional fluid mechanical model of near-instantaneous local equilibration of heat and momentum throughout the fluid follows from this, and provides a powerful tool for treating most macro scale flows. However, scale-separation is not always guaranteed in micro and nano scale flows: in these cases we often need to account for the effect of the fluid's molecular nature on the overall (macro) flow-field. Micro- and millisecond effects are important for micro and nano scale flows, but depend on the outcome of pico- or nanosecond molecular processes [3,4]. The design of future technologies that exploit micro and nano scale flow components will require the ability to resolve phenomena across scales of at least 8 orders of magnitude in space, and 10 orders of magnitude in time — a formidable multiscale problem.

In this paper we describe some of our most recent computational and theoretical tools we are bringing to bear on this problem. We examine slip flows in microscale gas and nanoscale liquid applications as quintessential non-equilibrium or sub-continuum phenomena that are still not properly understood. We

Copyright © 2011 by ASME

tackle gas and liquid flows alternately in this paper, because we wish to highlight the interesting commonalities between non-equilibrium gas and sub-continuum liquid flows at these small scales.

Thermodynamic non-equilibrium in gases

In dilute gas flows, molecules travel in free-flight between brief (binary) collisions with each other or bounding surfaces. The Knudsen number, Kn, indicates the degree of scale independence; in terms of the molecular mean-free-path, λ, and a characteristic length scale, L, of the system (or the local gradient of a relevant flow quantity, Q):

$$\mathrm{Kn} = \frac{\lambda}{L} \cong \frac{\lambda}{Q}\left|\frac{dQ}{dl}\right|. \qquad (1)$$

If $\mathrm{Kn} > 0.01$, physical scales are no longer clearly separated, and non-local-equilibrium flow behaviour arises: the flow velocity at a surface takes on a finite "slip" value, and the temperature of the gas near the surface also differs from the surface temperature. At higher Knthe linear NSF constitutive relations themselves become inappropriate. Air flowing at atmospheric pressures in a device with a characteristic length scale of 1μm has $\mathrm{Kn} \approx 0.1$ and will show these non-equilibrium (rarefaction) effects. Gas flows in, e.g., micro-pumps or micro-turbines of complex geometry will have a range of Kn: the NSF equations cannot, therefore, be expected to be generally applicable to these flows.

While a molecular-level description of the gas is available through the classical Boltzmann equation — or other kinetic models, such as BGK or ES-BGK — direct solution is computationally expensive. Even the cost of indirect methods, such as the direct simulation Monte Carlo (DSMC) technique, makes complex 3D full-field flow simulation impractical: to resolve micro flow velocities of the order of $0.01\,\mathrm{m/s}$ in DSMC, we need roughly 500 million statistical samples of the flowfield at any point [2]. However, variance reduction techniques can be applied to conventional DSMC to create a powerful and more economical method for generating molecular distributions at the most critical points in a flow.

A computationally-efficient gas flow method, but one which has had only modest success to date, is to establish either a Kn-series or a Hermite polynomial approximation to the distribution function in the Boltzmann equation. To first order, i.e. for near-equilibrium flows, both approaches yield the NSF set, but the solution methods can be continued to second and higher orders to incorporate more and more of the salient characteristics of a non-equilibrium flow. Specifying the additional boundary conditions required for the derived higher-moment and higher-order extended hydrodynamic equation sets remains a critical problem. In any case, the complexity of most of the models (Burnett, Grad 13-moment, R13, R26, etc.) is overwhelming, particularly when considering the only modest improvement in accuracy they provide. While they have particular difficulty in resolving strong non-equilibrium phenomena, e.g. the Knudsen layer close to bounding surfaces [5, 6], they may have some use in the "near near-equilibrium" regime [7, 8].

Thermodynamic non-equilibrium in liquids

Non-equilibrium phenomena analogous to that in gases (i.e. slip and non-linear constitutive behaviour) dominate liquid flows at the nanoscale. But identifying and modelling non-equilibrium in liquids is significantly more difficult than for gases: a Knudsen number cannot be ascribed because liquid molecules are constantly moving within each others' potentials, and the length scale for equilibrium breakdown is similar to that at which the continuum-fluid model itself fails. The complexity of material-dependent effects at interfaces cannot be treated by simple phenomenological parameters or by "equivalent fluxes" [9]. Direct molecular simulation of the liquid, however, can simultaneously model these phenomena with minimal simplifying assumptions, and some recent results will be presented below.

Molecular dynamics (MD) simulations calculate the intermolecular forces between molecules (based on their configuration in space) and then integrate the classical equations of motion using the net force on each molecule. Intermolecular force models can be empirically fitted to experimental data, or derived from first principles. The dynamics of real molecules in collision with real surfaces can then be investigated by accumulating the properties of individual molecules colliding with a (rough) surface lattice of molecules. The major problem again is that, like DSMC, MD is computationally very intensive. For example, to simulate $1\,\mu$s of water flow in a $10 \times 20 \times 100$nm channel would require up to 10 years on a modern PC. However, much of this time is spent in calculating unnecessary molecular detail in parts of the flow that are near to equilibrium [10]. Ultimately, a hybrid framework is called for, which dynamically couples the efficient NSF model in near-equilibrium regions to the detailed molecular dynamics model elsewhere.

MICRO GAS FLOWS

The problem of properly defining additional boundary conditions for extended hydrodynamics, as mentioned in the previous section, means that many rarefied and micro gas flow investigations are still conducted within the conventional NSF framework. However, there are still issues surrounding the correct implementation of non-equilibrium boundary conditions. To illustrate, we confine our attention here to models for calculating the slip-velocity to be imposed on hydrodynamic simulations of gas flows at solid bounding surfaces, although calculation of the temperature-jump at surfaces also requires careful consideration [11].

Copyright © 2011 by ASME

While there has been recent interest in using a Langmuir adsorption model of the gas/surface interaction to retrieve rarefied flow boundary conditions [12, 13], for flows of Kn > 0.001 Maxwell's phenomenological expression [14] remains the most often-used expression for the tangential slip-velocity, $\vec{u}_{\rm slip}$:

$$\vec{u}_{\rm slip} = -\frac{(2-\sigma)}{\sigma\mu}\lambda\,\vec{\tau} - \frac{3}{4}\frac{\Pr(\gamma-1)}{\gamma p}\vec{q}, \qquad (2)$$

where $\vec{\tau} = (\vec{i}_n \cdot \Pi)\cdot(\mathbf{1} - \vec{i}_n\vec{i}_n)$, $\vec{q} = \vec{Q}\cdot(\mathbf{1} - \vec{i}_n\vec{i}_n)$, an arrow denotes a vector quantity, σ is the momentum accommodation coefficient (equal to one for surfaces that reflect all incident molecules diffusely, and zero for purely specular reflection), μ is the gas viscosity at the wall, λ is the molecular mean-free-path at the wall, Pr is the Prandtl number, γ is the specific heat ratio, p is the gas pressure at the wall, $\vec{i}_n$ is a unit vector normal and away from the wall, Π is the stress tensor at the wall, $\mathbf{1}$ is the identity tensor and $\vec{Q}$ is the heat flux vector at the wall. Equation (2) is written in tensor form so that it is easily applicable to flows over three-dimensional surfaces

Because equation (2) requires the viscous-stress and heat-flux, we can choose to use the NSF constitutive expressions for these, as Maxwell himself did. For a flow bounded by planar surfaces (and for a perfect gas), we then obtain the conventional equation for the magnitude of the slip-velocity tangential to the surface, viz.

$$u_{\rm s} = \frac{(2-\sigma)}{\sigma}\lambda\frac{\partial u_x}{\partial n} + \frac{3}{4}\frac{\mu}{\rho T}\frac{\partial T}{\partial x}, \qquad (3)$$

where n is the coordinate normal to the wall, x is the coordinate tangential to the wall, u_x is the x-component of the gas velocity, $u_{\rm s}$ is the x-component of slip velocity, and ρ, T are the density and temperature of the gas at the wall, respectively.

While equation (3) has the advantage of simplicity, it should be remembered that it is incorrect for simulations of gas flows over curved or rotationally-moving surfaces, such as serpentine bends, spheres and cylinders, and other geometries in which the velocity normal to the surface varies in the streamwise direction (such as deflecting flaps). In such cases, using equation (3) instead of equation (2) misses out some important flow physics.

For example, Fig. 1 shows that the different boundary conditions produce radically different predictions of cylindrical micro Couette flow [15]. In this figure it is the inner cylinder that is rotating, but independent DSMC simulations show that the high gas velocities actually occur at the stationary outer cylinder wall. This curious rarefaction phenomenon is only captured by hydrodynamic models if the full Maxwell slip equation (2) is used, not the conventional slip equation (3). The no-slip fluid dynamic solution and an independent analytical result are also shown on this figure, for comparison. (Note that, for this flow system, differences in the results caused by using different boundary condition models are accentuated by the artificially low momentum accommodation coefficient.)

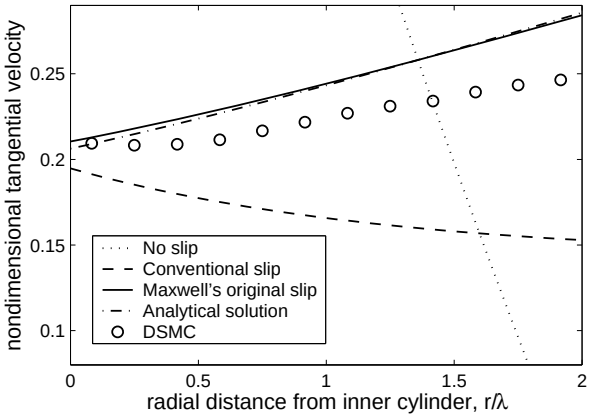

FIGURE 1. Cylindrical Couette flow (Kn $= 0.5$, argon gas), non-dimensional velocity radial profiles, comparing hydrodynamic solutions calculated using various slip-velocity models with benchmark DSMC data. The inner wall (at $r/\lambda = 0$) is rotating with a tangential velocity approximately a third the speed of sound relative to the outer wall (at $r/\lambda = 2$), the momentum accommodation coefficient is 0.1. Note the inverted velocity profile, captured by DSMC and an analytical kinetic theory but not by a hydrodynamic model (in this case, the NSF equations) unless the Maxwell original slip equation (2) is implemented properly in this curved geometry [15].

The conventional slip-velocity expression (3) is 1st-order in flow property gradients, but 2nd-order slip conditions have been proposed to account for the effect of Knudsen layers. The Knudsen layer is the region close to a solid surface over which the discontinuity introduced into the molecular distribution function by gas/surface interactions (with a surface usually modelled as a Maxwellian emitter) relaxes back to its bulk flow characteristic. This usually occurs over one or two mean-free-paths. Both momentum and thermal Knudsen layers occur generally in flows. While they exist close to surfaces in any gas flow, they only become important at the micro scale; in fact, for Kn > 0.1 they dominate the flow behaviour. Hydrodynamic models based on linear departures from local thermodynamic equilibrium, such as the NSF equations, cannot capture the non-linear Knudsen layer behaviour. Boundary conditions for the NSF equations can be set to compensate for the existence of a Knudsen layer through changing the magnitude of the slip-velocity, but they do not model the Knudsen layer structure itself.

A 2nd-order boundary condition formulation calculates a different magnitude for the slip-velocity (sometimes called a 'fictitious' slip-velocity) in an attempt to capture the increase in mass flowrates observed at higher Kn, but it cannot alter the near-wall stress/strain-rate (constitutive) behaviour which char-

Copyright © 2011 by ASME

acterises the Knudsen layer.

The general form of these 2nd-order conditions is, for planar surfaces,

$$u_s = A_1 \lambda \frac{\partial u_x}{\partial n} - A_2 \lambda^2 \frac{\partial^2 u_x}{\partial n^2}, \tag{4}$$

where we have also now assumed there is no heat flux along the surface. The values to be assigned to the coefficients A_1 and A_2 are still the subject of much discussion, and are in any case likely to be geometry-dependent [16].

While the form of equation (4) has been proposed because researchers wish to account for any unevaluated 2nd-order contributions to the slip-velocity, the original Maxwell slip condition (2) was proposed from physical considerations. Inspection of this equation, and its original derivation [14], shows that there is no *a priori* restriction on the expressions for the stress or heat-flux that it requires. While Maxwell used the NSF model, we are free to use another constitutive model; in [15] the Burnett extended hydrodynamic expression for the viscous-stress was used to derive a linearised 'Maxwell-Burnett' boundary condition, which is formally 2nd-order in space and stable in its solution. Expressing this new boundary condition in the form of equation (4) allows its coefficients A_1 and A_2 to be calculated: for a monatomic gas, $A_1 = 1.0$, $A_2 = 0.19$; for a diatomic gas, $A_1 = 1.0$, $A_2 = 0.145$ [16]. These values are generally in line with many of the other coefficient values proposed from theoretical or experimental considerations.

While the general problems with the Burnett equations are well-known, the justification for using them in this new 2nd-order boundary condition is that they may at least be better approximations than the NSF model for the non-equilibrium stress and heat-flux close to a surface. In fact, in [15] it was shown that the new Maxwell-Burnett boundary condition, applied with a conventional NSF hydrodynamic model for the bulk flow, generates a thermal-stress slip flow (as distinct from a thermal creep flow) when there is a tangential variation in the wall-normal temperature gradient. While this flow behaviour cannot be captured by Maxwell's boundary condition with an NSF model for the shear stress, its existence can be deduced from kinetic theory arguments.

The Maxwell-Burnett boundary condition has the advantage of relative simplicity because the Burnett equations provide an explicit expression for the viscous-stress, but in principle R13, R26 or other extended constitutive models with equation (2) would also be possible, and may shed new light on slip flows.

The NSF equations with slip boundary conditions are a surprisingly reasonable, as well as computationally-efficient, model in many micro gas flow cases. They should not be abandoned lightly in favour of far more complex extended hydrodynamic models. However, modifications to the NSF model can be made to incorporate some of the essential non-equilibrium behaviour near solid surfaces. While some accuracy (relative to extended hydrodynamics proper) is sacrificed in favour of ease of application, a major advantage of this approach to modelling non-equilibrium flows is that no additional boundary conditions beyond the slip/jump conditions outlined above are required.

This approach has been termed 'phenomenological extended hydrodynamics' (PEH). Borrowing an idea from the macroscale turbulence modelling community, PEH comprises a constitutive scaling of the NSF equations that depends on distance to a nearby solid surface. The physical basis for this constitutive scaling can be traced to the work of Stops [17], who demonstrated that the molecular mean-free-path of a gas is foreshortened (in comparison to its bulk flow value) close to an immovable solid surface. See also [18] for more recent work in this field. As the mean-free-path can be directly related to the viscosity and thermal conductivity of the gas, the fluid properties and behaviour of the gas some one to two mean-free-paths from a surface (i.e. in the Knudsen layer) are therefore expected to be different to those in the bulk flow.

Some of the most recent work in this field focuses on developing relatively simple analytical forms of the mean-free-path variation close to surfaces, from which non-linear constitutive relations can be straightforwardly derived. These modified NSF relations incorporate wall-distance scaling functions derived from planar kinetic theoretical results [1]. For example, for isothermal cases this scaling acts to change the form of the 3D low-speed steady-state incompressible NSF momentum equation to:

$$\nabla p = 2\mu \nabla \cdot (\Phi \overline{\nabla U}) = \mu \Phi \nabla^2 U + 2\mu \nabla \Phi \cdot \overline{\nabla U}, \tag{5}$$

where U is the gas flow velocity and $\overline{\nabla U} = [\nabla U + (\nabla U)^{\mathrm{T}}]/2$. The near-surface scaling function Φ in this equation is given by

$$\Phi = [1 + \Psi_1(\hat{n}) + K\Psi_2(\hat{n})]^{-1}, \tag{6}$$

where $\hat{n}$ is the perpendicular distance (nondimensionalised with λ) from the nearest wall surface [1].

Drawing on theoretical solutions of the Boltzmann equation for hard-sphere molecules, a power-law structure is an appropriate model of the inner part of the momentum Knudsen layer, with the consequence that the viscosity of the gas closest to the solid surface is effectively zero. This means that the test functions $\Psi_i(\hat{n})$ in equation (6) are of the form:

$$\Psi_i(\hat{n}) = a_i \hat{n}^{b_i} \exp\{c_i \hat{n}\}, \tag{7}$$

and a_i, b_i and c_i are coefficients that are determined once by op-

Copyright © 2011 by ASME

timisation from benchmark kinetic theory solutions to be:

$$a_1 = 0.1859,\ b_1 = -0.4640,\ c_1 = -0.7902; \qquad (8)$$
$$a_2 = 0.4205,\ b_2 = -0.3518,\ c_2 = -0.4521.$$

The flow-dependent variable, K, in equation (6) is in essence a form of local Knudsen number, and is introduced to provide a 2nd-order component to the constitutive scaling:

$$K = \frac{1}{\tau}\frac{d\tau}{d\hat{n}}, \qquad (9)$$

where the shear stress here, $\tau = \vec{i}_{\hat{x}} \cdot (\vec{i}_{\hat{n}} \cdot \Pi)$, has $\vec{i}_{\hat{n}}$ a unit vector in the wall-normal direction and $\vec{i}_{\hat{x}}$ a unit vector perpendicular to $\vec{i}_{\hat{n}}$ in a direction that gives maximum τ. This PEH model as a whole can indirectly (although will not necessarily) affect the shear stress field, which in turn will alter K, producing a weak coupling effect.

PEH equations are generally easy to incorporate into current computational fluid dynamics numerical codes and, despite their simplicity, their solutions are often in excellent agreement with a range of planar gas flow data (including Couette and Poiseuille flows). Perhaps surprisingly, given that the coefficients (8) for the test-functions are derived from planar kinetic theory results, PEH also shows good agreement in non-planar gas flow problems, such as the flow around a micro-sphere (see Fig. 2) [1]. It even shows moderate success when applied to high-speed thermal rarefied gas flows, e.g. in hypersonic aerothermodynamics [19], despite having mainly been derived for isothermal micro flows. In the form of effective mean-free-path models, near-wall scaling is also being introduced into lattice Boltzmann methods [16]. This seems to indicate a useful generality to the PEH technique which is worth exploring further.

While PEH offers some exciting new possibilities, and shows an ability to capture some essential features of non-equilibrium flows at the micro scale, it cannot be as accurate — in terms of recovering the detailed flow behaviour — as a comprehensive numerical or theoretical model based on the fundamental physics. For example, the simple wall-distance scaling models described above do not currently capture the bimodal temperature profile that is a prominent feature of force-driven Poiseuille flow. However, our view is that PEH fits into a hierarchy or 'spectrum' of simulation tools which the scientist or engineer can deploy on micro- or nano-flow problems, depending on the accuracy required of the result and the time allowed to achieve it.

At one end of this spectrum lie molecular techniques (such as DSMC), which produce very accurate results but are computationally expensive. At the other end of the spectrum lies the conventional NSF model, whose numerical solution for near-equilibrium engineering problems is now commonplace. Extended hydrodynamics lies between these two limits, with PEH lying towards the latter limit. Each method has its role and does not exclude any other, because each increases the choice of tools we can bring to bear on a particular flow problem.

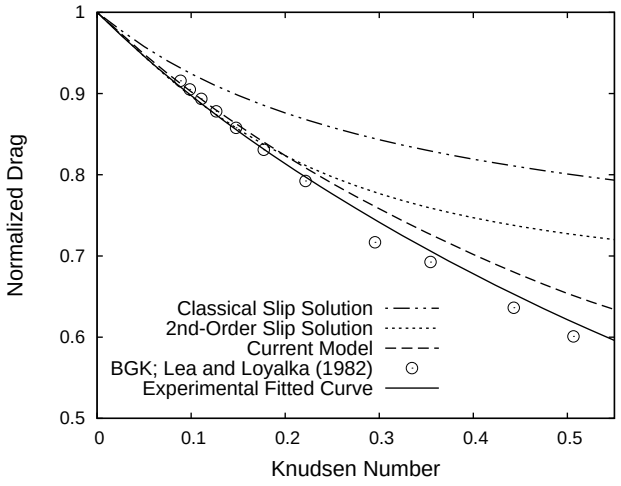

FIGURE 2. Flow around a sphere at various Kn, normalized drag force, comparing predictions using the near-wall constitutive scaling model of [1] with, as noted, Basset's classical slip solution, Cercignani's 2nd-order slip solution, BGK kinetic theory results, and experimental data. Of the hydrodynamic predictions shown, PEH shows by far the best agreement with experiment and kinetic theory up to Knudsen numbers beyond 0.5.

NANO LIQUID FLOWS

Slipping transport is also characteristic of water at the nanoscale. Recent experiments [20–22] and molecular dynamics (MD) simulations [23–26] have shown that water flows along carbon nanotubes (CNTs) at unexpectedly high rates. For CNTs of diameters below 1.66nm, the flow is 'non-continuum': the problem cannot be described using conventional continuum fluid mechanics even with modifications to the viscosity and slip boundary conditions [27]. Unlike the gas problems of the previous section — where reasonable solutions are obtainable by augmenting the correct slip boundary condition with a modified shear-stress/strain-rate relationship in the fluid close to a surface — the truly atomistic liquid transport problem requires a molecular dynamics simulation method.

Simulations of very small diameter CNTs show that the fluid forms single-file water molecule 'chains', where the movement of molecules is highly correlated and the water dipole moment is oriented in the direction of the flow [28]. This flow behaviour is not, however, observed in larger diameter CNTs: bulk-like flow structures are more typical. The flow rate decreases with decreasing CNT diameter, before increasing when approaching the

Copyright © 2011 by ASME

smallest diameters penetrable by water [23].

A single-walled CNT is essentially a sheet of graphene, rolled-up to form a cylinder or pipe; its morphology and diameter are specified by its chirality, generally expressed as a vector (*n*,*m*) that defines the position of the matched carbon rings during the roll-up. Previous studies have shown that there is no correlation between the CNT chirality and the internal fluid structure at CNT diameters below 1.66nm [23] therefore CNTs with different chiralities but the same diameter should produce similar results. In this paper we present our investigations of pressure-driven water flow through (7,7) CNTs, which have a diameter of 0.95 nm.

Molecular dynamics simulations

Our MD simulations were performed using `mdFoam` [3, 4, 10], a parallelised non-equilibrium molecular dynamics solver, that is open-source and available to download from the OpenFOAM website [29]. The motion of molecules in an MD simulation is governed by Newton's second law, and the equations of motion are integrated using the Verlet leapfrog scheme. A timestep of 1 fs is used in all the following simulations.

The rigid TIP4P water model is used, which consists of a Lennard-Jones (LJ) interaction potential at the oxygen atom site (O), positive Coulomb charges at the two hydrogen sites (H) and a negative charge at a site M, located a small distance away from O. The O-O LJ interactions use the following parameters: $\sigma_{OO} =$ 3.154 Å and $\varepsilon_{OO} = 0.6502$ kJ mol^{-1}. The electrostatic point charge values for water are -0.8476e and +0.4238e for the M and hydrogen sites, respectively. The carbon-water interaction is solely represented by a carbon-oxygen Lennard-Jones potential using the following parameters: $\sigma_{CO} = 3.19$ Å and $\varepsilon_{CO} = 0.392$ kJ mol^{-1} [30]. Electrostatic and Lennard-Jones interactions are smoothly truncated at 1.0nm.

The configuration of our pressure-driven flow simulation domain is shown in Fig. 3. Two graphene sheets are positioned at the inlet and outlet of the CNT to form a simplified membrane representation. The CNT and graphene sheets are modelled as rigid structures to speed up the MD runs. Periodic boundary conditions are employed in the *y*- and *z*-directions, while non-periodic boundary conditions are applied in the *x*-direction: the left-hand boundary is a specular-reflective wall, while the right-hand boundary deletes molecules upon collision. The wall helps control the fluid pressure and density upstream while the deletion patch creates an "open" system. We applied a pressure difference of 200 MPa across the membrane in all our simulations; such a large pressure difference is required to view the dynamics of the simulation over a shorter time period due to the large computational cost associated with MD. Berendsen thermostats are applied to both fluid reservoirs to maintain a constant temperature of 298 K and eliminate the contribution of any temperature gradients to the fluid transport. The fluid is not controlled inside the CNT so as not to disturb the dynamics of the contained water molecules.

The upstream pressure is controlled using a proportional-integral-derivative (PID) control feedback loop algorithm, similar to that used in [3], in addition to adaptive control of mass-flux at the inlet. An external force is distributed over all molecules which reside in control zone 1 to create the required pressure in the neighbouring sampling region, see Fig. 3. The required external force is calculated using three separate components: a proportional term, an integral term, and a derivative term. This type of technique is commonly used in modern feedback control systems.

A mass flux of water molecules is imposed at the inlet of the system in order to compensate for those molecules that leave the system, and to keep the upstream reservoir in a steady thermodynamic state. Our numerical implementation controls density adaptively in the inlet control zone: the target mass density in the control zone is set to the measured fluid density in the sampling region, because the pressure and temperature of the fluid in this region are set at the desired values. The pressure control process helps establish a steady, homogeneous density distribution because it forces molecules in and out of the control zone.

For molecule insertions, the USHER algorithm [31] is used, which searches for a site within the potential energy landscape via a steepest-descent iteration scheme. A molecule is inserted if the potential energy is equal to the cell-averaged potential energy. In this way, the algorithm ensures that the inserted molecule does not overlap with existing water molecules, nor does the local potential energy or temperature change after insertions/deletions. For deletion, the candidate molecule is chosen with its potential energy closest to the cell-averaged potential energy. Momentum and energy conservation steps are also performed after a molecule is inserted/deleted by distributing the added/removed momentum to neighbouring molecules, and updating the pair-forces.

The downstream pressure is controlled using a pressure-flux technique, which applies to all molecules in control zone 2 an external force that corresponds to the target pressure. By controlling pressure in this way, it creates an "open" boundary allowing a fluid flux to pass through the system [32]. A key advantage of our pressure control techniques is that the required reservoir pressures can be applied explicitly.

We investigate four different CNT lengths: 2.5, 5.0, 12.5, and 25nm. Initially the CNT is closed while the reservoirs are filled with water molecules and equilibrated to the correct conditions. After this initial equilibration, the CNT is opened and allowed to fill naturally. The system is then allowed to run for 250 ps before averaging of properties is performed. The same reservoir conditions are adopted in each simulation run.

Copyright © 2011 by ASME

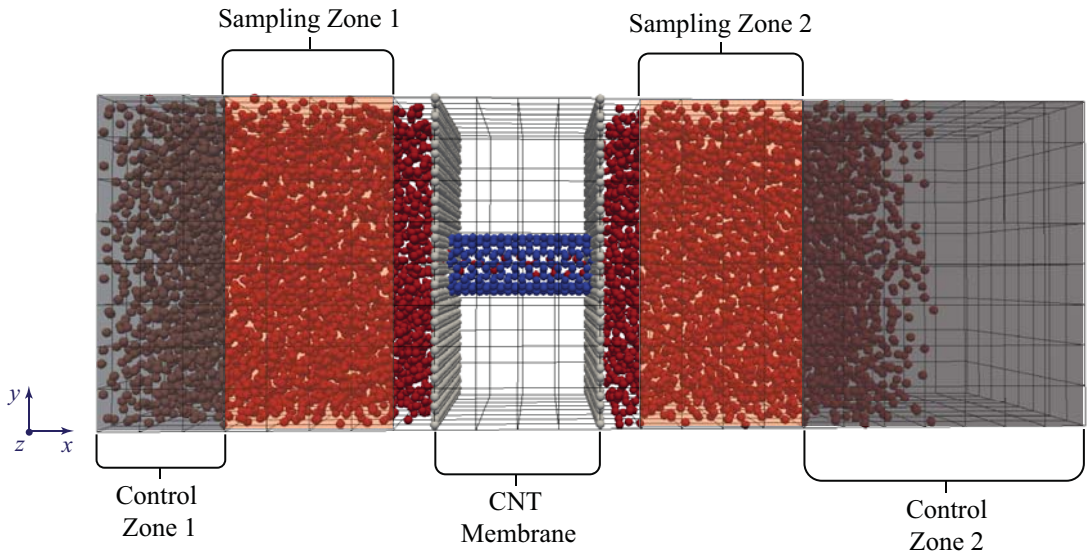

FIGURE 3. Domain for the molecular dynamics simulation of water transport in a carbon nanotube.

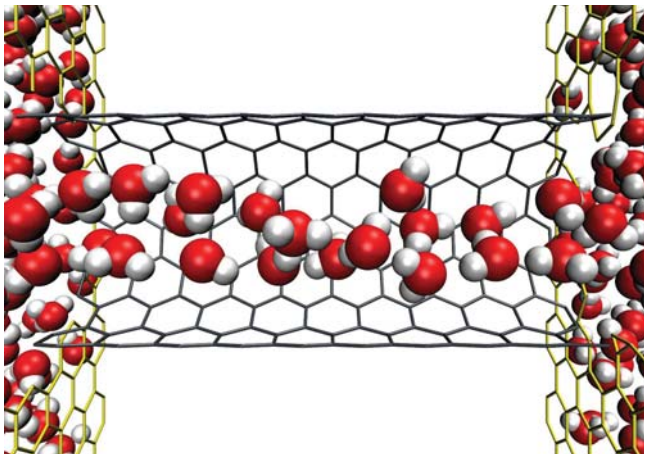

FIGURE 4. Molecular dynamics simulation of water molecules (red and white) transported through a short (7,7) carbon nanotube (green lines), shown in cutaway, that is fixed between two graphene membranes (thin gold lines). The water is moving from an upstream to a downstream reservoir.

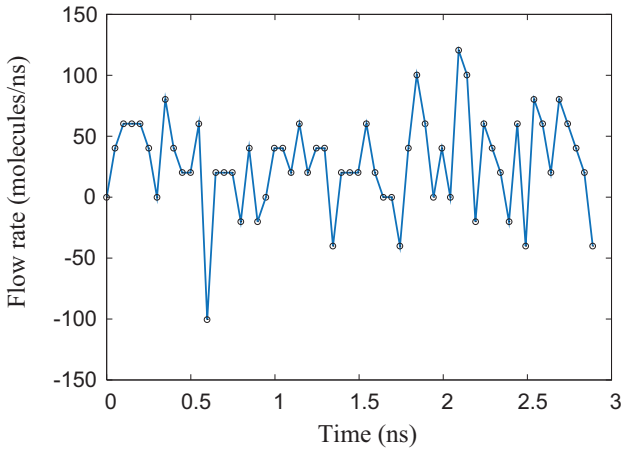

FIGURE 5. Flow rate through 2.5nm long CNT under 200 MPa pressure difference.

Fluid flow rate

As the fluid flow is non-continuum, the net flow rate is measured by averaging the number of molecules which cross five faces at different positions inside each CNT over a prescribed time period. The net flow rate for the 2.5nm long CNT measured over a 3ns time-period is shown in Fig. 5; each point on this graph is an average of 50,000 time steps. The flow rate fluctuates over a very short time period, reaching a maximum positive flow rate of 120 molecules/ns and a maximum negative value of 100 molecules/ns. The average flow rate is 32 molecules/ns in the positive direction, which gives an average mass flow rate of 9.57×10^{-16}kg/s. This value can be compared to the continuum flow rate calculated using the no-slip Poiseuille flow relation:

$$\dot{m} = \frac{\pi r^4 \rho \Delta P}{8 \mu L}, \tag{10}$$

where r is the radius of the CNT, ΔP is the pressure difference, ρ is the density, μ is the dynamic viscosity, and L is the CNT length. The radius used here is half of the carbon to carbon diameter less σ_{CO}. Using bulk properties for ρ and μ at 298 K, the flow enhancement factor, i.e. the ratio of the measured mass flow rate to the continuum prediction, is calculated to be 40.

The dynamic behaviour of the fluid in the CNT can also be seen in the individual water molecule trajectories. Figure 6

Copyright © 2011 by ASME

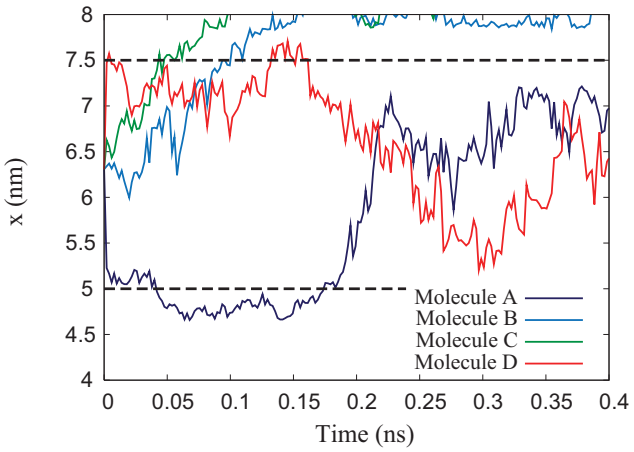

FIGURE 6. Individual molecular trajectories through a 2.5nm long CNT. Horizontal dashed lines indicate the positions of the CNT inlet and outlet.

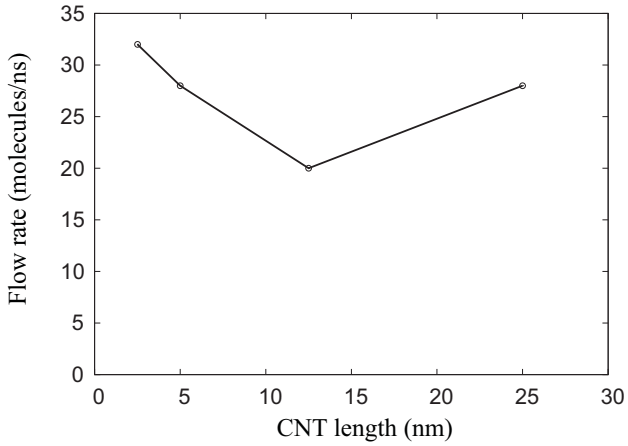

FIGURE 7. Relationship between water flow rate and CNT length under 200 MPa pressure difference.

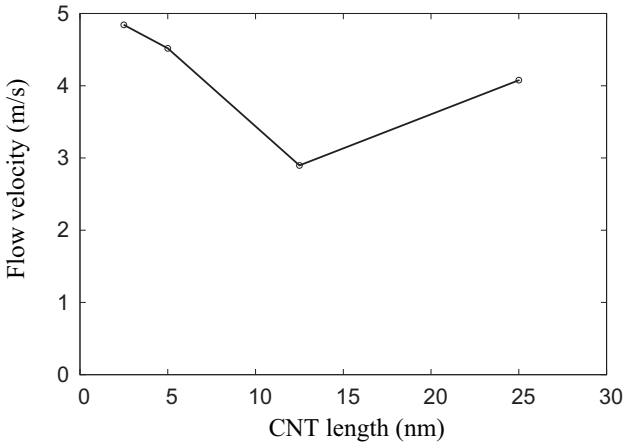

FIGURE 8. Variation of water flow velocity with CNT length under 200 MPa pressure difference.

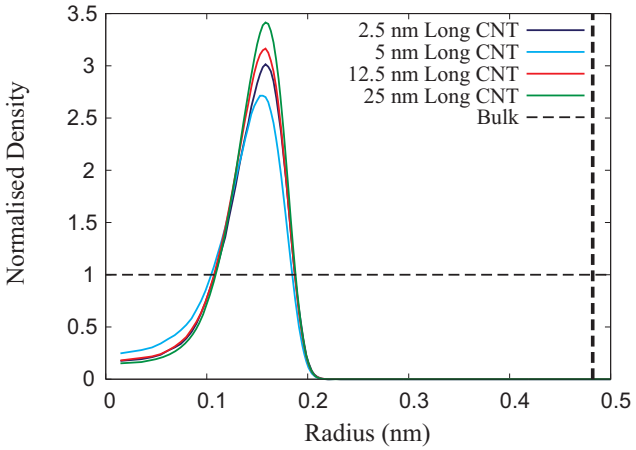

FIGURE 9. Water molecule radial density distributions, normalised with the reservoir density, for CNTs with different lengths. The average was performed over the entire length of the CNT. The vertical dashed line indicates the position of the CNT surface.

shows the axial trajectories of four water molecules, selected with different starting positions, as they pass through the CNT. The molecules can be seen to have both forwards and backwards motion.

The average net flow rate and flow velocity for the different nanotube lengths under the same applied pressure difference are shown in Fig. 7 and Fig. 8, respectively; each value was averaged over 1 ns (10^6 time steps). As the CNT length increases, both the flow rate and velocity decrease before increasing for the longest CNT. While there is a reduction of flow rate and velocity, the flow enhancement values increase to 71, 126, and 353 for the 5nm, 12.5nm and the 25nm lengths, respectively. This extraordinary non-continuum behaviour may be connected to the internal fluid structure, which is now described.

Radial density

The fluid structure within the CNTs is investigated by measuring the mean radial density. 300 cylindrical bins of equal volume and fixed length L_b are centred radially inside the CNT. The density within each bin is measured by summing the mass of the molecules contained over a specified period of time and dividing it by the bin length L_b and the number of averaging time-steps. The radial densities are measured at the inlet, centre, and outlet of each CNT, and over their entire lengths. Figure 9 shows that water contained within each CNT forms tightly packed cylindrical shells, whose densities are dependent upon CNT length. The density of water in the longer CNTs is greater than that of the shorter CNTs, with the 25nm long CNT having a maximum of almost 3.5 times that of the reservoir density. The distance be-

Copyright © 2011 by ASME

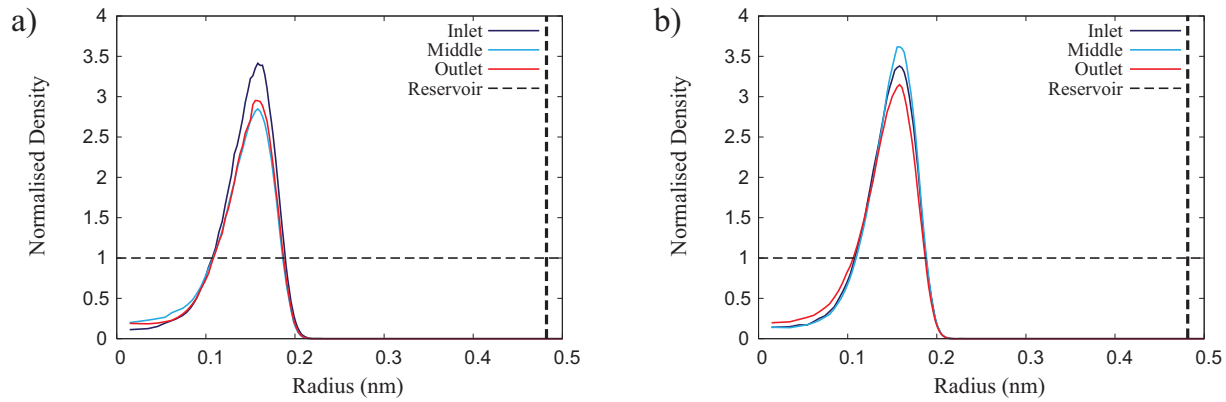

FIGURE 10. Water molecule radial density distributions normalised with the reservoir density at different locations along: a) 2.5nm long CNT and b) 25nm long CNT. The vertical dashed lines indicate the position of the CNT surfaces.

tween the peak density of the cylindrical shells and the CNT surface corresponds to the interaction length of the Lennard-Jones potential between the carbon and oxygen atoms, σ_{CO}.

Figure 10 shows how the radial density distribution varies at different positions along both the 2.5nm and 25nm CNTs. Both results show that the fluid structure is not uniform along either CNT. The density profiles are comparable at the inlet and outlet of each CNT which is expected since they are both connected to fluid reservoirs under identical conditions. However the density profiles measured at the centre of each CNT vary substantially: the density at the centre of the 25nm long CNT is much higher than that of the 2.5nm CNT. This indicates that the structure of the transported water is able to "develop" in longer CNTs i.e. CNTs with greater lengths optimise fluid structuring for significant flow rate enhancements.

CONCLUSIONS

The 21st century engineer will have to get used to counter-intuitive fluid flow behaviour at the micro- and nanoscale that has previously been the preserve of the physicist or physical chemist. Non-equilibrium/non-continuum behaviour is a major feature of both micro gas flows and nano liquid flows. In the case of slip, unless the correct model is used widely inaccurate results are obtained. In both cases, slip is not only a surface phenomenon — it extends into a gas flow as Knudsen layers, and into a liquid flow to structure the molecules nearby.

The example of water flow in CNTs is, perhaps, most instructive. It is first of all surprising that water molecules will enter and fill up such a narrow and hydrophobic tube, but molecular dynamics simulations show that filled CNTs are energetically preferred, because the CNT acts to structure the water molecules for the lowest potential energy. Water molecules inside a (7,7) CNT, which has a diameter of 0.95 nanometers, are organised in a tightly packed cylindrical shell, with densities reaching nearly four times that of the water outside the CNT. Our simulations show that, for the same pressure difference applied from end to end, longer CNTs have flow enhancements progressively above continuum expectations — most likely because longer CNTs act to structure the encapsulated water even more efficiently, and with greater densities. In smaller (6,6) CNTs, the water molecules even arrange themselves in single-file. It is as chains of molecules, suspended by intermolecular forces in the centre of the nanotube, that water is transported nearly frictionlessly along it. Conventional hydrodynamics, even incorporating a fluid/surface slip condition, cannot hope to capture such behaviour.

ACKNOWLEDGMENT

The authors would like to thank Rafael Delgado Buscalioni of the Universidad Autonoma de Madrid, and Matthew Borg of the University of Strathclyde for very useful discussions. The research leading to these results has received funding from the European Community's Seventh Framework Programme FP7/2007-2013 under grant agreement ITN GASMEMS no. 215504. JMR would also like to thank the Royal Academy of Engineering and the Leverhulme Trust for support through a Senior Research Fellowship.

REFERENCES

[1] Lockerby, D. A. and Reese, J. M., 2008, On the modelling of isothermal gas flows at the microscale, J. Fluid Mech., 604, 235-261.

[2] Reese, J. M., Gallis, M. A. and Lockerby, D. A., 2003, New directions in fluid dynamics: non-equilibrium aerodynamic and microsystem flows, Phil. Trans. Roy. Soc. A, 361, 2967-2988.

[3] Borg, M. K., Macpherson, G. B. and Reese, J. M., 2010, Controllers for imposing continuum-to-molecular bound-

Copyright © 2011 by ASME

ary conditions in arbitrary fluid flow geometries, Mol. Sim., 36, 745-757.
[4] Macpherson, G. B. and Reese, J. M., 2008, Molecular dynamics in arbitrary geometries: parallel evaluation of pair forces, Mol. Sim., 34, 97-115.
[5] Lockerby, D. A., Reese, J. M. and Gallis, M. A., 2005, The usefulness of higher-order constitutive relations for describing the Knudsen layer, Phys. Fluids, 17, 100609.
[6] Lockerby, D. A., Reese, J. M. and Gallis, M. A., 2005, Capturing the Knudsen layer in continuum-fluid models of non-equilibrium gas flows, AAIA J., 43, 1391-1393.
[7] Lockerby, D. A., Reese, J. M. and Struchtrup, H., 2009, Switching criteria for hybrid rarefied gas flow solvers, Proc. Roy. Soc. A, 465, 1581-1598.
[8] Gu, X. J. and Emerson, D. R., 2009, A high-order moment approach for capturing non-equilibrium phenomena in the transition regime, J. Fluid Mech., 636, 177-216.
[9] Brenner, H. and Ganesan, V., 2000, Molecular wall effects: are conditions at a boundary boundary conditions? Phys. Rev. E, 61, 6879-6897.
[10] Macpherson, G. B. and Reese, J. M., 2006, Molecular dynamics for near surface flows in nano liquid and micro gas systems, 4th ASME Intl Conf Nanochannels, Microchannnels & Minichannels, ICNMM2006, 96170.
[11] O'Hare, L., Scanlon, T. J., Emerson, D. R. and Reese, J. M., 2008, Evaluating constitutive scaling models for application to compressible microflows, Int. J. Heat Mass Transf., 51, 1281-1292.
[12] Myong, R. S., Reese, J. M., Barber, R. W. and Emerson, D. R., 2005, Velocity slip in microscale cylindrical Couette flow: the Langmuir model, Phys. Fluids, 17, 087105.
[13] Myong, R. S., Lockerby, D. A. and Reese, J. M., 2006, The effect of gaseous slip on microscale heat transfer: an extended Graetz problem, Int. J. Heat Mass Transf., 49, 2502-2513.
[14] Maxwell, J. C., 1879, On stresses in rarified gases arising from inequalities of temperature, Philos. Trans. Roy. Soc., Part 1, 170, 231-256.
[15] Lockerby, D. A., Reese, J. M., Emerson, D. R. and Barber R. W., 2004, Velocity boundary condition at solid walls in rarefied gas calculation, Phys. Rev. E, 70, 017303.
[16] Reese, J. M. and Zhang, Y. H., 2009, Simulating fluid flows in micro and nano devices: the challenge of non-equilibrium behaviour, J. Computat. Theoret. Nanosci., 6, 2061-2074.
[17] Stops, D. W., 1970, The mean free path of gas molecules in the transition regime, J. Phys. D: Appl. Phys., 3, 685-696.
[18] Dongari, N., Zhang Y. H. and Reese, J. M., 2011, Molecular free path distribution in rarefied gases, J. Phys. D: Appl. Phys., 44, 125502.
[19] Lofthouse, A. J., Scalabrin, L. C. and Boyd, I. D., 2008, Velocity slip and temperature jump in hypersonic aerothermodynamics, J. Thermophys. Heat Transf., 22, 38-49.
[20] Majumder, M., Chopra, N., Andrew, R. and Hinds, B. J., 2005, Nanoscale hydrodynamics: enhanced flow in carbon nanotubes, Nature, 438, 44.
[21] Holt, J. K., Park, H. G., Wang, Y., Stadermann, M., Artyukhin, A. B., Grigoropoulos, C. P., Noy, A. and Bakajin, O., 2006, Fast mass transport through sub-2-nanometer carbon nanotubes, Science, 312, 1034-1037.
[22] Whitby, M., Cagnon, L., Thanou, M. and Quirke, N., 2008, Enhanced fluid flow through nanoscale carbon pipes, Nano Lett., 8, 2632-2637.
[23] Thomas, J. A., McGaughey, A. J. H. and Kuter-Arnebeck, O., 2010, Pressure-driven water flow through carbon nanotubes: insights from molecular dynamics simulation, Int. J. Therm. Sci., 49, 281-289.
[24] Corry, B., 2008, Designing carbon nanotube membranes for efficient water desalination, J. Phys. Chem. B, 112, 1427-1434.
[25] Joseph, S. and Aluru, N. R., 2008, Why are carbon nanotubes fast transporters of water? Nano Lett., 8, 452-458.
[26] Suk, M. E., Raghunathan, A. V. and Aluru, N. R., 2008, Fast reverse osmosis using boron nitride and carbon nanotubes, App. Phys. Lett., 92, 133120.
[27] Thomas, J. A. and McGaughey, A. J. H., 2009, Water flow in carbon nanotubes: transition to subcontinuum transport, Phys. Rev. Lett., 102, 184502.
[28] Wan, R., Lu, H., Li, J., Bao, J., Hu, J. and Fang, H., 2009, Concerted orientation induced unidirectional water transport through nanochannels, Phys. Chem. Chem. Phys., 11, 9898-9902.
[29] http://www.openfoam.com (March 29, 2011)
[30] Werder, T., Walther, J. H., Jaffe, R., Halicioglu, T. and Koumoutsakos, P., 2003, On the water-carbon interaction for use in molecular dynamics simulations of graphite and carbon nanotubes, J. Phys. Chem. B, 107, 1345-1352.
[31] DeFabritiis, G., Delgado-Buscalioni, R. and Coveney, P. V., 2004, Energy controlled insertion of polar molecules in dense fluids, J. Chem. Phys., 121, 12139-12142.
[32] Delgado-Buscalioni, R., Kremer, K. and Praprotnik, M., 2009, Coupling atomistic and continuum hydrodynamics through a mesoscopic model: application to liquid water, J. Chem. Phys., 131, 244107.

Copyright © 2011 by ASME